Relation between the areal rate of Zitterbewegung and Berry curvature in two-band systems

Sonja Predin *

Institute of Physics Belgrade, University of Belgrade, Pregrevica 118, 11080 Belgrade, Serbia

(Received 11 April 2026; revised 14 August 2026; accepted 18 September 2026; published 7 October 2026)

We introduce the *Zitterbewegung areal rate* operator to study the relation between the orientation of trembling motion and band topology. Constructed from the oscillatory interband displacement and velocity, this operator distinguishes clockwise from anticlockwise motion. For a generic gapped two-band Hamiltonian in two dimensions, we show that the Zitterbewegung areal rate is proportional to the Berry curvature. The derivation uses only spectral projectors and is therefore gauge invariant. We also demonstrate that the Zitterbewegung areal rate operator is time independent and a constant of motion at each momentum, although the displacement and velocity from which it is constructed oscillate in time. Its sign distinguishes anticlockwise from clockwise Zitterbewegung and coincides with the sign of the Berry curvature. For wave packets narrowly localized around the isolated massive Dirac points, the Zitterbewegung chirality equals the sign of the local Chern contribution. The Chern number can therefore be reconstructed from the orientations of the Zitterbewegung motion around the individual Dirac points.

DOI: 10.1103/pt3n-gym8

I. INTRODUCTION

The geometry of Bloch states in momentum space is encoded in the quantum geometric tensor, whose real and imaginary parts determine the quantum metric and the Berry curvature, respectively. In two dimensions, the integral of the Berry curvature over the Brillouin zone is related to the first Chern number [1,2]. The Berry curvature also governs anomalous transport and orbital magnetic responses [2–4], while the quantum metric contributes to the superfluid weight of multiband superconductors [5] and to the stability of fractional Chern-insulator states [6]. Band geometry also manifests itself in real-time dynamics. In particular, wave-packet motion has been used to probe the Berry curvature and the topology of Bloch bands [7,8].

Zitterbewegung is an important quantum-dynamical phenomenon that arises from interference between different energy bands. It was first predicted by Schrödinger for relativistic electrons governed by the Dirac equation [9]. Schliemann *et al.* later showed that an analogous motion in spin-orbit-coupled semiconductors arises from interband mixing [10]. Zitterbewegung has since been studied in graphene [11,12], carbon nanotubes [13], ultracold atoms [14], Weyl semimetals [15], semiconductors [16,17], topological insulators [18,19], and twisted bilayer systems [20].

Zitterbewegung provides a natural setting for studying the relation between interband dynamics and the geometry and topology of individual Bloch bands. Previous studies have shown that wave-packet and Zitterbewegung dynamics can carry topological information. In particular, Li *et al.* demonstrated that the center-of-mass motion of a wave packet, containing both directed and transient Zitterbewegung contributions, can reveal the chirality of a Weyl point [15]. Moreover, Liu *et al.* experimentally observed valley dependent self-rotation of photonic wave packets and related it theoretically to Zitterbewegung oscillations [21]. More directly related to the present work, Shen *et al.* showed that the orientation of Zitterbewegung trajectories in spin-J Dirac models depends on the valley index and the sign of the mass term, which changes across a band inversion, thereby relating Zitterbewegung to band topology [17].

Motivated by these results, we introduce a new quantity, which we call the *areal rate of Zitterbewegung*, to characterize Zitterbewegung chirality. Since chirality distinguishes clockwise from anticlockwise motion, this quantity should change sign when the orientation of the trajectory is reversed. A natural choice is therefore an antisymmetric combination of position and velocity. At fixed momentum $\mathbf{k}$, we denote the field-free interband oscillatory part of Heisenberg position operator by $\delta\hat{\mathbf{r}}(\mathbf{k}, t)$ and define

$$\widehat{\mathcal{R}}_{\mathrm{ZB}}(t) = \tfrac{1}{2}[\delta r_x(t)\,\delta\dot{r}_y(t) - \delta r_y(t)\,\delta\dot{r}_x(t)]. \tag{1}$$

In this paper, we establish an exact analytical relation between band geometry, specifically the Berry curvature, and Zitterbewegung in generic two-band system in two dimensions

$$\widehat{\mathcal{R}}_{\mathrm{ZB}}(\mathbf{k}) = \frac{\omega(\mathbf{k})}{2}\Omega_-(\mathbf{k})\,\mathbb{I}, \tag{2}$$

where $\omega(\mathbf{k}) = E_+(\mathbf{k}) - E_-(\mathbf{k}) > 0$ is the frequency of the interband Zitterbewegung motion, $\Omega_-(\mathbf{k})$ is the Berry curvature of the lower band, and we set $\hbar = 1$. The derivation is written entirely in terms of spectral projectors and does not require a particular gauge choice for the Bloch eigenstates. Although the position and velocity operators oscillate in time, their time dependence cancels in the antisymmetric product. The areal rate operator is therefore time independent, and a constant of motion at fixed momentum. Moreover, because it

*Contact author: sonja@ipb.ac.rs

 ©2026 American Physical Society

is proportional to the identity, its expectation value does not depend on the initial internal two-component state.

Furthermore, since $\omega(\mathbf{k}) > 0$, the areal rate has the same sign as the local Berry curvature. The chirality of the Zitterbewegung motion is therefore determined by the sign of the Berry curvature, consistent with the valley and mass dependent direction of the motion found by Liu *et al.* and Shen *et al.* [17,21]. In the two-dimensional two-band models considered here, the same parameters also determine the sign of the Berry curvature, suggesting a connection between Zitterbewegung chirality and local band geometry. In this paper, we make this connection explicit by introducing the *areal rate of Zitterbewegung*, a gauge-invariant signed quantity that characterizes the orientation of the interband motion.

Since Zitterbewegung center-of-mass dynamics is already experimentally accessible in photonic and ultracold atom systems, this reconstruction could be implemented by resolving the orientation of the motion near the individual Dirac points [22–24].

The paper is organized as follows. In Sec. II, we formulate the interband Zitterbewegung dynamics using spectral projectors. In Sec. III, we introduce the *areal rate of Zitterbewegung*, derive its exact relation to the Berry curvature for a generic two-band Hamiltonian, and extend the result to wave packets. We then relate the Zitterbewegung chirality near a massive Dirac point to its contribution to the Chern number and illustrate the result using a two-dimensional Chern insulator model. We close with a summary and an outlook in Sec. IV. Technical details of the derivation are given in Appendix A.

II. ZITTERBEWEGUNG IN PROJECTOR FORM

In this paper, we mainly consider a generic two-band Hamiltonian $\mathcal{H}(\mathbf{k})$. However, it is useful to begin with the general spectral-projector representation. We impose the two-band restriction explicitly below, at the point where it becomes necessary. Throughout the paper, we set $\hbar \equiv 1$.

In the Heisenberg picture, the position operator for generic Hamiltonian $\mathcal{H}(\mathbf{k})$ evolves as [25]

$$\hat{\mathbf{r}}(t) = e^{i\mathcal{H}t}\,\hat{\mathbf{r}}(0)\,e^{-i\mathcal{H}t}. \tag{3}$$

We use the spectral (projector) decomposition

$$\mathcal{H}(\mathbf{k}) = \sum_a E_a(\mathbf{k})\,Q_a(\mathbf{k}), \tag{4}$$

where the projectors Q_a are Hermitian, mutually orthogonal, and complete,

$$Q_a Q_b = \delta_{ab} Q_a \tag{5}$$

and

$$\sum_a Q_a = \mathbb{I}. \tag{6}$$

Using this decomposition, the position operator separates into an intraband drift term and an interband oscillatory contribution,

$$\hat{\mathbf{r}}(t) = \hat{\mathbf{r}}(0) + t\sum_a \mathbf{V}_a Q_a + \sum_{a\neq b}(e^{i\omega_{ab}t} - 1)\mathbf{Z}_{ab}, \tag{7}$$

where $\mathbf{Z}_{ab} = iQ_a\partial_{\mathbf{k}}Q_b$ encode interband Zitterbewegung oscillations at frequencies $\omega_{ab} = E_a - E_b$, and $\mathbf{V}_a = \partial E_a/\partial\mathbf{k}$ denotes the band-group velocity. Thus, the Zitterbewegung contribution arises from the interband terms $Q_a\partial_{k_i}Q_b$ with $a \neq b$.

For the analysis below, we consider only the Zitterbewegung contribution and rewrite it as

$$\delta\hat{r}_i(t) = \sum_{a\neq b} e^{i\omega_{ab}t} Z^i_{ab}. \tag{8}$$

The time-independent term $-\sum_{a\neq b} Z^i_{ab}$ in Eq. (7) represents a constant displacement of the center of the oscillatory motion and is neglected together with the remaining nonoscillatory part of the position operator.

We now restrict the analysis to a two-band Hamiltonian. Denoting the two bands by $+$ and $-$, Eq. (8) becomes

$$\begin{aligned}\delta\hat{r}_i(t) = {}& i(Q_+\partial_{k_i}Q_- + Q_-\partial_{k_i}Q_+)\cos(\omega t)\\ & - (Q_+\partial_{k_i}Q_- - Q_-\partial_{k_i}Q_+)\sin(\omega t),\end{aligned} \tag{9}$$

where $\omega = E_+(\boldsymbol{k}) - E_-(\boldsymbol{k})$.

Any Hermitian two-band Bloch Hamiltonian can be written as in the terms of Pauli matrices σ_i

$$\mathcal{H}(\mathbf{k}) = d_0(\mathbf{k})\mathbb{I} + \mathbf{d}(\mathbf{k})\cdot\boldsymbol{\sigma}. \tag{10}$$

The scalar term $d_0(\mathbf{k})\mathbb{I}$ affects only the intraband drift, shifts the energy bands, and leaves the topology unchanged. Since we are interested in the interband Zitterbewegung contribution, we set $d_0 = 0$ and write

$$\mathcal{H}(\mathbf{k}) = \sum_{i=1}^{3} d_i(\mathbf{k})\,\sigma_i, \tag{11}$$

with eigenvalues $E_\pm = \pm d$, where $d = \sqrt{d_1^2 + d_2^2 + d_3^2}$. The gap closes at points where $\boldsymbol{d}(\mathbf{k}) = 0$.

Introducing $\hat{\mathbf{d}} = \mathbf{d}/d$, the corresponding spectral projectors are

$$Q_\pm = \tfrac{1}{2}(\mathbb{I} \pm \hat{\mathbf{d}}\cdot\boldsymbol{\sigma}). \tag{12}$$

Substituting these projectors into Eq. (9), we obtain

$$\begin{aligned}\delta\hat{r}_i(t) = {}& \tfrac{1}{2}(\hat{\mathbf{d}}\times\partial_{k_i}\hat{\mathbf{d}})\cdot\boldsymbol{\sigma}\,\cos(\omega t)\\ & + \tfrac{1}{2}(\partial_{k_i}\hat{\mathbf{d}})\cdot\boldsymbol{\sigma}\,\sin(\omega t),\end{aligned} \tag{13}$$

with $\omega = 2d$. This expression makes explicit that the Zitterbewegung dynamics are determined by the momentum space texture of the unit vector $\hat{\mathbf{d}}$.

The same spectral projectors provide a gauge-invariant representation of the Berry curvature. For an isolated band a, the Berry curvature is

$$\Omega^{(a)}_{\alpha\beta}(\mathbf{k}) = i\,\mathrm{tr}[Q_a[\partial_{k_\alpha}Q_a, \partial_{k_\beta}Q_a]], \tag{14}$$

while the corresponding quantum metric is

$$g^{(a)}_{\alpha\beta}(\mathbf{k}) = \tfrac{1}{2}\,\mathrm{tr}[\partial_{k_\alpha}Q_a\partial_{k_\beta}Q_a]. \tag{15}$$

These expressions are invariant under local gauge transformations of the Bloch eigenstates because they are written entirely in terms of the spectral projector Q_a, rather than a particular choice of the corresponding eigenvector [26].

For a two-band Hamiltonian in two dimensions in Eq. (11), substituting projectors Eq. (12) into Eqs. (14) and (15) for lower band − gives

$$\Omega^{(-)}_{\alpha\beta}(\mathbf{k}) = \tfrac{1}{2}\,\hat{\mathbf{d}}\cdot\left(\partial_{k_\alpha}\hat{\mathbf{d}}\times\partial_{k_\beta}\hat{\mathbf{d}}\right) \tag{16}$$

and

$$g^{(-)}_{\alpha\beta}(\mathbf{k}) = \tfrac{1}{4}\partial_{k_\alpha}\hat{\mathbf{d}}\cdot\partial_{k_\beta}\hat{\mathbf{d}}. \tag{17}$$

Thus, the Zitterbewegung dynamics, the Berry curvature, and the quantum metric are all determined by the momentum-space texture of $\hat{\mathbf{d}}(\mathbf{k})$.

III. AREAL RATE OF ZITTERBEWEGUNG AND BERRY CURVATURE

Recent photonic studies have demonstrated wave-packet motion with a well-defined sense of rotation associated with Zitterbewegung in symmetry broken honeycomb lattices and a synthetic Weyl system [21,27]. In symmetry broken honeycomb photonic lattices, Liu *et al.* experimentally observed valley dependent wave packet self-rotation in the form of spiraling intensity patterns [21]. Their theoretical analysis related this self-rotation to Zitterbewegung oscillations of the wave-packet center of mass, with a frequency determined by the spectral gap. In a theoretical study of a synthetic Weyl system, Ye *et al.* found helical Zitterbewegung near a Weyl point and related it to the non-Abelian Berry connection [27].

Related theoretical work has connected the orientation of Zitterbewegung motion to band inversion. For spin-J models, Shen *et al.* showed that changing the sign of the effective mass term across a gap closing reverses the orientation of the Zitterbewegung trajectory [17].

Motivated by these results, we introduce a dynamical observable that characterizes the orientation of interband Zitterbewegung. We show that, for a generic two-band Hamiltonian in two dimensions, this observable is directly related to the Berry curvature.

Let $\delta\hat{\mathbf{r}}(t)$ denote the interband oscillatory part of the Heisenberg position operator introduced above. In two dimensions, a combination of this displacement and its velocity gives the quantum analogue of the area sweep rate. We define the corresponding time-dependent quantity

$$\widehat{\mathcal{R}}_{\mathrm{ZB}}(t) = \tfrac{1}{2}[\delta r_x(t)\,\delta\dot{r}_y(t) - \delta r_y(t)\,\delta\dot{r}_x(t)]. \tag{18}$$

We call this quantity the *Zitterbewegung areal rate*.

Its sign distinguishes clockwise from anticlockwise motion, while its magnitude gives the corresponding areal rate. We consider a two-band system, where a single interband pair gives the full Zitterbewegung motion. In this case, we show that the Zitterbewegung areal rate is directly related to the Berry curvature. The oscillatory coordinate obeys

$$\delta\dot{\hat{\mathbf{r}}}(t) = i[\mathcal{H}, \delta\hat{\mathbf{r}}(t)]. \tag{19}$$

This definition is similar to the intrinsic self-rotation of a semiclassical Bloch wave packet, described by $\frac{1}{2}\langle(\hat{\mathbf{r}}-\mathbf{r}_c)\times\hat{\mathbf{v}}\rangle$ and related to its orbital magnetic moment [2]. There is, however, an important difference. In the semiclassical approach, the wave packet is constructed within a single isolated band. In contrast, $\widehat{\mathcal{R}}_{\mathrm{ZB}}$ is defined from the exact interband part of the Heisenberg position operator.

As shown below, for a two-band Hamiltonian, $\widehat{\mathcal{R}}_{\mathrm{ZB}}$ is directly proportional to the Berry curvature, with the interband frequency as the proportionality factor. The exact identity derived here is specific to gapped two-band Hamiltonians.

Moreover, the operator $\widehat{\mathcal{R}}_{\mathrm{ZB}}$ is Hermitian, since $[\delta\hat{x}, \delta\dot{\hat{y}}] = [\delta\hat{y}, \delta\dot{\hat{x}}]$, and therefore its expectation value is real.

Substituting Eq. (9) into Eq. (18) and using the orthogonality of the projectors, we find that all time-dependent terms cancel, leaving

$$\widehat{\mathcal{R}}_{\mathrm{ZB}} = i\frac{\omega}{2}\Bigg[Q_a\frac{\partial Q_b}{\partial k_x}\frac{\partial Q_a}{\partial k_y} - Q_a\frac{\partial Q_b}{\partial k_y}\frac{\partial Q_a}{\partial k_x} - Q_b\frac{\partial Q_a}{\partial k_x}\frac{\partial Q_b}{\partial k_y} + Q_b\frac{\partial Q_a}{\partial k_y}\frac{\partial Q_b}{\partial k_x}\Bigg]. \tag{20}$$

For a two-band system, the completeness relation $Q_+ + Q_- = \mathbb{I}$ then gives

$$\widehat{\mathcal{R}}_{\mathrm{ZB}}(\mathbf{k}) = i\frac{\omega}{2}Q_-\left[\frac{\partial Q_-}{\partial k_x}, \frac{\partial Q_-}{\partial k_y}\right] - i\frac{\omega}{2}Q_+\left[\frac{\partial Q_+}{\partial k_x}, \frac{\partial Q_+}{\partial k_y}\right]. \tag{21}$$

The derivation is given in Appendix A.

For a two-band Hamiltonian holds $Q_a = |u_a\rangle\langle u_a|$, and therefore, for any operator X, we have

$$Q_a X Q_a = \langle u_a|X|u_a\rangle Q_a = \mathrm{Tr}(Q_a X)\,Q_a. \tag{22}$$

Setting

$$X = i\left[\frac{\partial Q_a}{\partial k_x}, \frac{\partial Q_a}{\partial k_y}\right] \tag{23}$$

and using the definition of the Berry curvature Eq. (14), we obtain

$$iQ_a\left[\frac{\partial Q_a}{\partial k_x}, \frac{\partial Q_a}{\partial k_y}\right]Q_a = \Omega_a Q_a. \tag{24}$$

Multiplying Eq. (21) from the right by Q_- and Q_+, respectively, and adding the resulting expressions, we obtain

$$\widehat{\mathcal{R}}_{\mathrm{ZB}}(\mathbf{k}) = \frac{\omega(\mathbf{k})}{2}\Omega_-(\mathbf{k})\,\mathbb{I}. \tag{25}$$

A derivation of Eq. (25) is given in Appendix A.

Equation (25) gives an exact local relation between interband Zitterbewegung and the Berry curvature. The sign of the Zitterbewegung areal rate is fixed by the sign of the Berry curvature and determines the orientation of the motion.

Cserti and Dávid [28] expressed the Berry curvature in terms of the amplitudes Z_{aa} with equal band indices. Since $\omega_{aa} = 0$, these amplitudes do not describe oscillatory motion and give no contribution to the Zitterbewegung areal rate. In contrast, the areal rate in Eq. (25) is constructed from the interband amplitudes Z_{ab}, with $a \neq b$, which enter the position operator through terms oscillating at frequencies $\omega_{ab} = E_a - E_b$.

Another consequence of Eq. (25) is that the Zitterbewegung areal rate is a constant of motion. Although the Zitterbewegung position operator oscillates in time, $\widehat{\mathcal{R}}_{\mathrm{ZB}}$ is time independent and proportional to the identity operator. It therefore commutes with the Hamiltonian,

$$\left[\mathcal{H}(\mathbf{k}), \widehat{\mathcal{R}}_{\mathrm{ZB}}(\mathbf{k})\right] = 0, \tag{26}$$

and hence

$$\frac{d}{dt}\widehat{\mathcal{R}}_{\mathrm{ZB}}(\mathbf{k}) = i\big[\mathcal{H}(\mathbf{k}), \widehat{\mathcal{R}}_{\mathrm{ZB}}(\mathbf{k})\big] = 0. \tag{27}$$

Thus, at each momentum $\mathbf{k}$, the areal rate remains constant even though the Zitterbewegung position oscillates. This result is specific to the two-band case.

To connect the momentum-resolved result with wave-packet dynamics, we consider a Gaussian wave packet centered at a band-inversion point, which we take as the origin of momentum space, $\mathbf{k}_0 = 0$:

$$|\psi(\mathbf{r}, 0)\rangle = \frac{1}{\sqrt{\pi}\,\Delta} \exp\left(-\frac{x^2 + y^2}{2\Delta^2}\right)|\Phi\rangle. \tag{28}$$

Here, Δ is the real-space width of the wave packet and $|\Phi\rangle$ is its normalized initial pseudospin state. The corresponding normalized momentum-space distribution is

$$G_{\mathbf{k}_0}(\mathbf{k}) = \frac{\Delta^2}{\pi} \exp(-\Delta^2 k^2), \quad \int d^2\mathbf{k}\, G(\mathbf{k}) = 1. \tag{29}$$

Thus, in the large Δ limit, the momentum distribution becomes sharply localized around the band-inversion point. Since Δ is the real-space width, the corresponding momentum-space width is of order $1/\Delta$. The single-cone approximation is valid when this width is much smaller than the distance to the other Dirac points and the packet remains within the momentum region where the linearized Dirac Hamiltonian applies. This condition is required only for the wave-packet application; the exact local identity in Eq. (25) is independent of Δ.

We parametrize the pseudospin state as

$$|\Phi\rangle = a\,|1, 0\rangle + b\,|0, 1\rangle, \tag{30}$$

corresponding to the eigenbasis of σ_z. The choice of quantization axis is conventional and does not affect the generality of the results.

For a wave packet centered at $\mathbf{k}_0$, we define the wave-packet averaged Zitterbewegung areal rate as

$$\mathcal{R}^{\mathrm{wp}}_{\mathrm{ZB}}(\mathbf{k}_0) = \int d^2\mathbf{k}\, G_{\mathbf{k}_0}(\mathbf{k}) \big\langle \widehat{\mathcal{R}}_{\mathrm{ZB}}(\mathbf{k}) \big\rangle. \tag{31}$$

Using Eq. (25), we obtain

$$\mathcal{R}^{\mathrm{wp}}_{\mathrm{ZB}}(\mathbf{k}_0) = \frac{1}{2} \int d^2\mathbf{k}\, G_{\mathbf{k}_0}(\mathbf{k})\, \omega(\mathbf{k})\, \Omega_-(\mathbf{k}). \tag{32}$$

Since $\widehat{\mathcal{R}}_{\mathrm{ZB}}$ is proportional to the identity matrix, this result does not depend on the initial pseudospin state $|\Phi\rangle$.

For the two-band Hamiltonian introduced in Eq. (10), the areal rate can also be written as

$$\mathcal{R}^{\mathrm{wp}}_{\mathrm{ZB}} = \frac{1}{4} \int d^2\mathbf{k}\, G_{\mathbf{k}_0}(\mathbf{k})\, \omega(\mathbf{k})\, \hat{\mathbf{d}} \cdot \big(\partial_{k_x}\hat{\mathbf{d}} \times \partial_{k_y}\hat{\mathbf{d}}\big). \tag{33}$$

For the same two-band system, the Berry curvature and the quantum metric satisfy

$$\det g(\mathbf{k}) = \tfrac{1}{4}\Omega_-^2(\mathbf{k}). \tag{34}$$

Using this relation, the wave-packet areal rate can also be written as

$$\mathcal{R}^{\mathrm{wp}}_{\mathrm{ZB}} = \int d^2\mathbf{k}\, G_{\mathbf{k}_0}(\mathbf{k})\, \omega(\mathbf{k})\, \mathrm{sgn}[\Omega_-(\mathbf{k})] \sqrt{\det g(\mathbf{k})}. \tag{35}$$

Thus, the magnitude of the local areal rate depends on the quantum metric, while the Berry curvature determines the direction of the Zitterbewegung motion. This equality is specific to two-band Hamiltonians in two dimensions and follows from the Pauli-matrix algebra, or equivalently from the mapping of the Bloch states to the Bloch sphere [29]. It does not generally hold as an equality in multiband systems.

For a two-band Hamiltonian each Dirac point D contributes to the Chern number. The contribution is determined by the chirality η_D of the Dirac point and the sign of its mass m_D [30]:

$$\mathrm{Ch}_- = \sum_D \mathrm{Ch}_D, \quad \mathrm{Ch}_D = \tfrac{1}{2}\eta_D \mathrm{sgn}(m_D). \tag{36}$$

Here,

$$m_D = d_3(D), \tag{37}$$

$$\eta_D = \mathrm{sgn}(J_D), \quad J_D = [\partial_{k_x}\mathbf{d} \times \partial_{k_y}\mathbf{d}]_3\big|_{\mathbf{k}=\mathbf{D}}. \tag{38}$$

Moreover,

$$\mathrm{sgn}[\Omega_-(D)] = \eta_D \mathrm{sgn}(m_D) = \mathrm{sgn}(\mathrm{Ch}_D). \tag{39}$$

For a wave packet narrowly centered at $\mathbf{D}$ and sampling Berry curvature of a single sign, we define

$$\chi^D_{\mathrm{ZB}} \equiv \mathrm{sgn}\big(\mathcal{R}^{\mathrm{wp},D}_{\mathrm{ZB}}\big) = \mathrm{sgn}(\mathrm{Ch}_D). \tag{40}$$

Here, χ^D_{ZB} denotes the Zitterbewegung chirality and specifies the orientation of the motion. The values $\chi^D_{\mathrm{ZB}} = +1$ and -1 correspond to anticlockwise and clockwise motion, respectively. The Chern number can therefore be reconstructed from the orientation of the Zitterbewegung motion around the individual Dirac points:

$$\mathrm{Ch}_- = \frac{1}{2}\sum_D \chi^D_{\mathrm{ZB}}. \tag{41}$$

The Chern-number reconstruction in Eq. (41) is consistent with the relation between local Zitterbewegung directions and topological invariants found by Shen *et al.* for spin-J Dirac models [17].

For a fixed Dirac-point chirality, a band inversion changes the sign of the mass, thereby reversing both the Berry curvature and the direction of the Zitterbewegung rotation. The Zitterbewegung areal rate thus provides a direct dynamical signature of the underlying band topology. For a sufficiently narrow wave packet with nonzero interband coherence, the areal rate of the center-of-mass trajectory has the same sign as the expectation value of the Zitterbewegung areal-rate operator, although the two quantities generally differ in magnitude.

Zitterbewegung has already been observed in photonic systems and ultracold atomic gases by tracking the wave-packet center-of-mass [22–24]. For an interband-coherent wave packet prepared near a massive Dirac point, measuring both components of this motion would show whether the trajectory is clockwise or anticlockwise. Its orientation would determine χ^D_{ZB} and directly test the relation between Zitterbewegung chirality and the local Berry curvature.

Chern-insulator model

We finally illustrate our result using a two-dimensional Chern insulator model on a square lattice. The model supports both trivial and Chern-insulating phases. Setting the lattice constant to unity, the Bloch Hamiltonian reads

$$\mathcal{H}(\boldsymbol{k}) = A(\sin k_x\, \sigma_x + \sin k_y\, \sigma_y) + m(\boldsymbol{k})\sigma_z, \tag{42}$$

$$m(\boldsymbol{k}) = M - 2B(2 - \cos k_x - \cos k_y), \tag{43}$$

where $A = \pm 1$, B, and M are real model parameters. The corresponding band energies are

$$E_{\pm}(\boldsymbol{k}) = \pm d(\boldsymbol{k}), \tag{44}$$

where

$$d(\boldsymbol{k}) = \sqrt{A^2(\sin^2 k_x + \sin^2 k_y) + m^2(\boldsymbol{k})}. \tag{45}$$

Moreover, the model exhibits four Dirac points $D \in \langle \Gamma,\, X,\, Y,\, \mathrm{M} \rangle$,

$$\begin{aligned} \Gamma &= (0,0), \quad X = (\pi, 0), \\ Y &= (0,\pi), \quad \mathrm{M} = (\pi,\pi). \end{aligned} \tag{46}$$

The low-energy Hamiltonian near each of these points $\mathbf{k} = D + \mathbf{q}$ has the following form,

$$\mathcal{H}_D(\boldsymbol{q}) = A\left(v_x^D q_x\, \sigma_x + v_y^D q_y\, \sigma_y\right) + m_D \sigma_z\,, \tag{47}$$

where m_D are corresponding mass terms

$$m_\Gamma = M, \quad m_X = m_Y = M - 4B, \quad m_{\mathrm{M}} = M - 8B. \tag{48}$$

Furthermore, the chirality of each Dirac cone is determined by

$$\eta_D \equiv \mathrm{sgn}\left(v_x^D v_y^D\right), \tag{49}$$

where $v_x^D = \cos(D_x)$ and $v_y^D = \cos(D_y)$. Therefore,

$$\eta_\Gamma = \eta_{\mathrm{M}} = +1, \quad \eta_X = \eta_Y = -1. \tag{50}$$

In this case, the dispersion relation becomes

$$E_{\pm}^D(\boldsymbol{q}) = \pm\sqrt{m_D^2 + A^2 q^2}, \tag{51}$$

so that the interband frequency is $\omega_D(\boldsymbol{q}) = 2\sqrt{m_D^2 + A^2 q^2}$.

The low-energy Berry curvature for lower band in the vicinity of D is

$$\Omega_-^D(\boldsymbol{q}) = \frac{\eta_D A^2 m_D}{2\left(m_D^2 + A^2 q^2\right)^{3/2}}. \tag{52}$$

The corresponding Dirac-cone contribution to the Chern number is

$$\begin{aligned} \mathrm{Ch}_D &\equiv \frac{1}{2\pi}\int_{\mathbb{R}^2} d^2\boldsymbol{q}\, \Omega_-^D(\boldsymbol{q}) \\ &= \frac{\eta_D}{2}\mathrm{sgn}(m_D). \end{aligned} \tag{53}$$

Thus, Ch_D represents the half-integer contribution of an individual continuum Dirac cone, whereas only the sum of all Dirac-cone contributions gives the integer Chern number of the lattice model.

Substituting the low-energy dispersion relation, Eq. (51), and the Berry curvature near the Dirac point D, Eq. (52), into the general relation (25), we obtain the Zitterbewegung areal rate operator near D:

$$\begin{aligned} \widehat{\mathcal{R}}_{\mathrm{ZB}}^D(\boldsymbol{q}) &= \frac{\omega_D(\boldsymbol{q})}{2}\Omega_-^D(\boldsymbol{q})\,\mathbb{I} \\ &= \frac{\eta_D A^2 m_D}{2\left(m_D^2 + A^2 q^2\right)}\,\mathbb{I}. \end{aligned} \tag{54}$$

Consequently, for a normalized momentum distribution $G_D(\boldsymbol{q})$ localized around D, we obtain

$$\mathcal{R}_{\mathrm{ZB}}^{\mathrm{wp},D} \simeq \int d^2\boldsymbol{q}\, G_D(\boldsymbol{q})\, \frac{\eta_D A^2 m_D}{2\left(m_D^2 + A^2 q^2\right)}. \tag{55}$$

Finally, the local Zitterbewegung chirality near the Dirac points has the following form:

$$\begin{aligned} \chi_{\mathrm{ZB}}^D &\equiv \mathrm{sgn}\left(\mathcal{R}_{\mathrm{ZB}}^{\mathrm{wp},D}\right) \\ &= \eta_D \mathrm{sgn}(m_D) = \mathrm{sgn}(\mathrm{Ch}_D) = 2\,\mathrm{Ch}_D. \end{aligned} \tag{56}$$

At $m_D = 0$, the gap closes and the Zitterbewegung chirality is undefined.

Figure 1 illustrates that, for fixed Dirac-point chirality $\eta_D = 1$, a band inversion reverses the sign of the Berry curvature near the Dirac point and, consequently, the orientation of the Zitterbewegung motion. This orientation is determined by $\chi_{\mathrm{ZB}}^D = \mathrm{sgn}(\mathcal{R}_{\mathrm{ZB}}^{\mathrm{wp},D})$, with $\chi_{\mathrm{ZB}}^D = +1$ (-1) corresponding to anticlockwise (clockwise) motion.

For a Dirac cone with $\eta_D = -1$, the signs of χ_{ZB}^D and the corresponding orientations shown in Fig. 1 are reversed.

The Chern number of the lower band is obtained by summing the four Dirac cone contributions

$$\begin{aligned} \mathrm{Ch}_- &= \frac{1}{2\pi}\int_{\mathrm{BZ}} d^2\boldsymbol{k}\, \Omega_-(\boldsymbol{k}) \\ &= \frac{1}{2}\sum_D \chi_{\mathrm{ZB}}^D \\ &= \frac{1}{2}[\mathrm{sgn}(M) - 2\mathrm{sgn}(M - 4B) + \mathrm{sgn}(M - 8B)]. \end{aligned} \tag{57}$$

For $B > 0$, the resulting Chern numbers and local Zitterbewegung chiralities are summarized in Table I.

TABLE I. Chern number and Zitterbewegung chirality at the Dirac points for $B > 0$.

M	$M < 0$	$0 < M < 4B$	$4B < M < 8B$	$M > 8B$
Ch	0	1	−1	0
$\chi_{\mathrm{ZB}}^{\Gamma}$	−	+	+	+
χ_{ZB}^{X}	+	+	−	−
χ_{ZB}^{Y}	+	+	−	−
$\chi_{\mathrm{ZB}}^{\mathrm{M}}$	−	−	−	+

The results explicitly demonstrate that the Zitterbewegung chirality at each Dirac point directly reflects its local topological charge, while the sum of the individual contributions reconstructs the total Chern number.

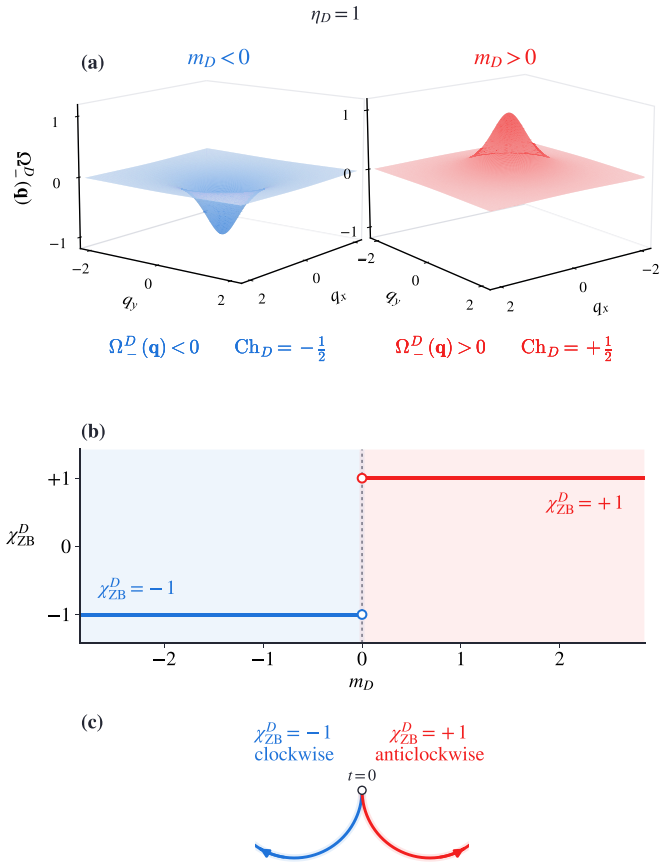

FIG. 1. Relation between the Dirac mass, Berry curvature, and Zitterbewegung chirality near a Dirac point. For a fixed Dirac-point chirality $\eta_D = +1$, the sign of the Dirac mass m_D determines the signs of the Berry curvature Ω_-^D and the local Chern contribution Ch_D. (a) Berry curvature near the Dirac point for $m_D < 0$ and $m_D > 0$. (b) The Zitterbewegung chirality $\chi_{\mathrm{ZB}}^D = \mathrm{sgn}(\mathrm{Ch}_D)$ changes sign with m_D and is undefined at $m_D = 0$, where the gap closes. (c) Schematic Zitterbewegung trajectories illustrating the corresponding change from clockwise to anticlockwise motion.

IV. CONCLUSIONS

We have introduced the Zitterbewegung areal rate to characterize the orientation of Zitterbewegung motion. For a generic gapped two-dimensional two-band Hamiltonian, we derived an exact relation between the areal rate and the Berry curvature. We have demonstrated that the Zitterbewegung areal rate operator is time independent, although the displacement and velocity from which it is constructed oscillate in time. The resulting operator is proportional to the identity and is a constant of motion at each momentum, independent of the initial internal state.

The sign of the areal rate coincides with that of the lower-band Berry curvature and distinguishes anticlockwise from clockwise Zitterbewegung. For wave packets narrowly localized around isolated massive Dirac points, the Zitterbewegung chirality therefore reproduces the sign of the corresponding local Chern contribution. Consequently, the Chern number can be reconstructed from the orientations of the Zitterbewegung motion around the individual Dirac points in the two-dimensional two-band system.

The exact operator identity derived in this work applies to gapped two-band Hamiltonians in two dimensions. The multiband case requires a separate analysis and is outside the scope of the present work.

The relation derived here could be tested in photonic or ultracold atom systems by preparing an interband coherent wave packet near a massive Dirac point and determining whether its motion is clockwise or anticlockwise.

ACKNOWLEDGMENTS

The author acknowledges funding provided by the Institute of Physics Belgrade through a grant from the Ministry of Science, Technological Development and Innovation of the Republic of Serbia. I am grateful to F. Mireles for helpful correspondence and comments on an earlier version of the manuscript.

DATA AVAILABILITY

There are no publicly available research data or software supporting this manuscript. Requests for further information or data should be sent to the author.

APPENDIX: DERIVATION OF THE ZITTERBEWEGUNG AREAL-RATE IDENTITY

In this Appendix, we derive Eqs. (21) and (25) from the definition of the Zitterbewegung areal rate in Eq. (18). For compactness, we introduce the shorthand notation

$$A_i = Q_a \partial_{k_i} Q_b, \quad B_i = Q_b \partial_{k_i} Q_a, \tag{A1}$$

where the band labels are chosen such that $\omega = E_a - E_b > 0$. The oscillatory position operator in Eq. (9) can then be written as

$$\delta\hat{r}_i(t) = i(A_i + B_i)\cos(\omega t) - (A_i - B_i)\sin(\omega t). \tag{A2}$$

Substituting Eq. (A2) and its time derivative into Eq. (18), we obtain

$$\begin{aligned}\widehat{\mathcal{R}}_{\mathrm{ZB}} = {} & \frac{\omega}{2}\left[A_x A_y - A_y A_x + B_x B_y - B_y B_x\right]\sin(2\omega t) \\ & + i\frac{\omega}{2}\left[A_x B_y - A_y B_x - B_x A_y + B_y A_x\right] \\ & - i\frac{\omega}{2}\left[A_x A_y - A_y A_x - B_x B_y + B_y B_x\right]\cos(2\omega t).\end{aligned} \tag{A3}$$

Differentiating the orthogonality relation $Q_a Q_b = 0$ for $a \neq b$ gives

$$\frac{\partial Q_a}{\partial k_i} Q_b = -Q_a \frac{\partial Q_b}{\partial k_i} \tag{A4}$$

and differentiating the projector identity $Q_a^2 = Q_a$ gives

$$\frac{\partial Q_a}{\partial k_i} Q_a = \frac{\partial Q_a}{\partial k_i} - Q_a \frac{\partial Q_a}{\partial k_i}. \tag{A5}$$

These relations imply

$$A_iA_j = -Q_aQ_b\frac{\partial Q_a}{\partial k_i}\frac{\partial Q_b}{\partial k_j}, \tag{A6}$$

$$B_iB_j = -Q_bQ_a\frac{\partial Q_b}{\partial k_i}\frac{\partial Q_a}{\partial k_j}, \tag{A7}$$

$$A_iB_j = Q_a\frac{\partial Q_b}{\partial k_i}Q_b\frac{\partial Q_a}{\partial k_j}, \tag{A8}$$

$$B_iA_j = Q_b\frac{\partial Q_a}{\partial k_i}Q_a\frac{\partial Q_b}{\partial k_j}. \tag{A9}$$

Using the orthogonality relation $Q_aQ_b = 0$ once again, we obtain

$$A_iA_j = 0, \tag{A10}$$

$$B_iB_j = 0, \tag{A11}$$

$$A_iB_j = Q_a\frac{\partial Q_b}{\partial k_i}\frac{\partial Q_a}{\partial k_j}, \tag{A12}$$

$$B_iA_j = Q_b\frac{\partial Q_a}{\partial k_i}\frac{\partial Q_b}{\partial k_j}. \tag{A13}$$

Consequently, all terms proportional to $\sin(2\omega t)$ and $\cos(2\omega t)$ in Eq. (A3) vanish, leaving

$$\widehat{\mathcal{R}}_{\mathrm{ZB}} = i\frac{\omega}{2}\Big(Q_a\frac{\partial Q_b}{\partial k_x}\frac{\partial Q_a}{\partial k_y} - Q_a\frac{\partial Q_b}{\partial k_y}\frac{\partial Q_a}{\partial k_x} - Q_b\frac{\partial Q_a}{\partial k_x}\frac{\partial Q_b}{\partial k_y} + Q_b\frac{\partial Q_a}{\partial k_y}\frac{\partial Q_b}{\partial k_x}\Big). \tag{A14}$$

Thus, the areal rate associated with a fixed interband pair is time independent.

For a two-band system, where $a = +$ and $b = -$, this is the full Zitterbewegung contribution. Using $Q_+ + Q_- = \mathbb{I}$, and hence $\partial_{k_i}Q_+ = -\partial_{k_i}Q_-$, Eq. (A14) reduces to Eq. (21) of the main text

$$\widehat{\mathcal{R}}_{\mathrm{ZB}}(\mathbf{k}) = i\frac{\omega}{2}Q_-\left[\frac{\partial Q_-}{\partial k_x}, \frac{\partial Q_-}{\partial k_y}\right] - i\frac{\omega}{2}Q_+\left[\frac{\partial Q_+}{\partial k_x}, \frac{\partial Q_+}{\partial k_y}\right]. \tag{A15}$$

For a two-band Hamiltonian, the spectral projectors are given by

$$Q_a = |u_a\rangle\langle u_a|. \tag{A16}$$

Therefore, for any operator X,

$$\begin{aligned} Q_aXQ_a &= |u_a\rangle\langle u_a|X|u_a\rangle\langle u_a| \\ &= \langle u_a|X|u_a\rangle Q_a \\ &= \mathrm{Tr}(Q_aX)\,Q_a. \end{aligned} \tag{A17}$$

Setting

$$X = i[\partial_{k_x}Q_a, \partial_{k_y}Q_a] \tag{A18}$$

we find

$$iQ_a[\partial_{k_x}Q_a, \partial_{k_y}Q_a]Q_a = \Omega_aQ_a. \tag{A19}$$

Furthermore, we multiply Eq. (21) by Q_- and, after some algebra, obtain

$$\widehat{\mathcal{R}}_{\mathrm{ZB}}Q_- = \omega\Omega_-Q_- - i\frac{\omega}{2}\left[\frac{\partial Q_-}{\partial k_x}, \frac{\partial Q_-}{\partial k_y}\right]Q_-. \tag{A20}$$

Analogously, multiplying Eq. (21) by Q_+, we obtain

$$\widehat{\mathcal{R}}_{\mathrm{ZB}}Q_+ = -\omega\Omega_+Q_+ + i\frac{\omega}{2}\left[\frac{\partial Q_+}{\partial k_x}, \frac{\partial Q_+}{\partial k_y}\right]Q_+. \tag{A21}$$

Since $\partial_{k_i}Q_+ = -\partial_{k_i}Q_-$, the two commutators are equal. Furthermore, the commutator $[\partial_{k_i}Q_a, \partial_{k_j}Q_a]$ commutes with Q_a. Adding Eqs. (A20) and (A21) and using Eq. (21), we obtain

$$\widehat{\mathcal{R}}_{\mathrm{ZB}} = \omega\Omega_-Q_- - \omega\Omega_+Q_+ - \widehat{\mathcal{R}}_{\mathrm{ZB}}. \tag{A22}$$

Finally, using $\Omega_+ = -\Omega_-$ and $Q_+ + Q_- = I$, we find

$$\widehat{\mathcal{R}}_{\mathrm{ZB}}(\mathbf{k}) = \frac{\omega(\mathbf{k})}{2}\Omega_-(\mathbf{k})I. \tag{A23}$$

[1] D. J. Thouless, M. Kohmoto, M. P. Nightingale, and M. den Nijs, Quantized Hall conductance in a two-dimensional periodic potential, Phys. Rev. Lett. **49**, 405 (1982).

[2] D. Xiao, M.-C. Chang, and Q. Niu, Berry phase effects on electronic properties, Rev. Mod. Phys. **82**, 1959 (2010).

[3] N. Nagaosa, J. Sinova, S. Onoda, A. H. MacDonald, and N. P. Ong, Anomalous Hall effect, Rev. Mod. Phys. **82**, 1539 (2010).

[4] X.-B. Qiang, T. Liu, H.-Z. Lu, and X. C. Xie, Quantum geometric origin of orbital magnetization, Appl. Phys. Lett. **128**, 010501 (2026).

[5] S. Peotta and P. Törmä, Superfluidity in topologically nontrivial flat bands, Nat. Commun. **6**, 8944 (2015).

[6] S. A. Parameswaran, R. Roy, and S. L. Sondhi, Fractional Chern insulators and the W_{inf} algebra, Phys. Rev. B **85**, 241308(R) (2012).

[7] M. Aidelsburger, M. Atala, M. Lohse, J. T. Barreiro, B. Paredes, and I. Bloch, Realization of the Hofstadter Hamiltonian with ultracold atoms in optical lattices, Phys. Rev. Lett. **111**, 185301 (2013).

[8] N. Fläschner, B. S. Rem, M. Tarnowski, D. Vogel, D.-S. Lühmann, K. Sengstock, and C. Weitenberg, Experimental reconstruction of the Berry curvature in a Floquet Bloch band, Science **352**, 1091 (2016).

[9] E. Schrödinger, Über die kräftefreie Bewegung in der relativistischen Quantenmechanik, Sitzungsber. Preuss. Akad. Wiss. Phys. Math. Kl **24**, 418 (1930).

[10] J. Schliemann, D. Loss, and R. M. Westervelt, Zitterbewegung of electronic wave packets in III-V zinc-blende semiconductor quantum wells, Phys. Rev. Lett. **94**, 206801 (2005).

[11] T. M. Rusin and W. Zawadzki, Zitterbewegung of electrons in graphene in a magnetic field, Phys. Rev. B **78**, 125419 (2008).
[12] A. Santacruz, P. E. Iglesias, R. Carrillo-Bastos, and F. Mireles, Valley-driven Zitterbewegung in Kekulé-distorted graphene, Phys. Rev. B **105**, 205405 (2022).
[13] W. Zawadzki, One-dimensional semirelativity for electrons in carbon nanotubes, Phys. Rev. B **74**, 205439 (2006).
[14] J. Y. Vaishnav and C. W. Clark, Observing Zitterbewegung in ultracold atoms, Phys. Rev. Lett. **100**, 153002 (2008).
[15] Z. Li, H.-Q. Wang, D.-W. Zhang, S.-L. Zhu, and D.-Y. Xing, Dynamics of Weyl quasiparticles in an optical lattice, Phys. Rev. A **94**, 043617 (2016).
[16] J. Schliemann, D. Loss, and R. M. Westervelt, Zitterbewegung of electrons and holes in III-V semiconductor quantum wells, Phys. Rev. B **73**, 085323 (2006).
[17] X. Shen, Y.-Q. Zhu, and Z. Li, Link between Zitterbewegung and topological phase transitions, Phys. Rev. B **106**, L180301 (2022).
[18] B. Dóra, J. Cayssol, F. Simon, and R. Moessner, Optically engineering the topological properties of a spin Hall insulator, Phys. Rev. Lett. **108**, 056602 (2012).
[19] L. K. Shi, S. C. Zhang, and K. Chang, Anomalous electron trajectory in topological insulators, Phys. Rev. B **87**, 161115(R) (2013).
[20] I. R. Lavor, D. R. da Costa, L. Covaci, M. V. Milošević, F. M. Peeters, and A. Chaves, Zitterbewegung of moiré excitons in twisted MoS_2/WSe_2 heterobilayers, Phys. Rev. Lett. **127**, 106801 (2021).
[21] X. Liu, F. Lunić, D. Song, Z. Dai, S. Xia, L. Tang, J. Xu, Z. Chen, and H. Buljan, Valley-dependent wavepacket self-rotation and Zitterbewegung in symmetry- broken honeycomb lattices, Laser Photonics Rev. **15**, 2000563 (2021).
[22] S. Lovett, P. M. Walker, A. Osipov, A. Yulin, P. U. Naik, C. E. Whittaker, I. A. Shelykh, M. S. Skolnick, and D. N. Krizhanovskii, Observation of Zitterbewegung in photonic microcavities, Light Sci. Appl. **12**, 126 (2023).
[23] L. J. LeBlanc, M. C. Beeler, K. Jiménez-García, A. R. Perry, S. Sugawa, R. A. Williams, and I. B. Spielman, Direct observation of Zitterbewegung in a Bose-Einstein condensate, New J. Phys. **15**, 073011 (2013).
[24] C. Qu, C. Hamner, M. Gong, C. Zhang, and P. Engels, Observation of Zitterbewegung in a spin-orbit-coupled Bose-Einstein condensate, Phys. Rev. A **88**, 021604(R) (2013).
[25] G. Dávid and J. Cserti, General theory of Zitterbewegung, Phys. Rev. B **81**, 121417(R) (2010).
[26] J. Mitscherling, A. Avdoshkin, and J. E. Moore, Gauge-invariant projector calculus for quantum state geometry and applications to observables in crystals, Phys. Rev. B **112**, 085104 (2025).
[27] W. Ye, Y. Liu, J. Liu, S. A. R. Horsley, S. Wen, and S. Zhang, Photonic Hall effect and helical Zitterbewegung in a synthetic Weyl system, Light: Sci. Appl. **8**, 49 (2019).
[28] J. Cserti and G. Dávid, Relation between Zitterbewegung and the charge conductivity, Berry curvature, and the Chern number of multiband systems, Phys. Rev. B **82**, 201405(R) (2010).
[29] B. Mera, A. Zhang, and N. Goldman, Relating the topology of Dirac Hamiltonians to quantum geometry: When the quantum metric dictates Chern numbers and winding numbers, SciPost Phys. **12**, 018 (2022).
[30] D. Sticlet, F. Piéchon, J.-N. Fuchs, P. Kalugin, and P. Simon, Geometrical engineering of a two-band Chern insulator in two dimensions with arbitrary topological index, Phys. Rev. B **85**, 165456 (2012).